

Self-Supervised Action-Space Prediction for Automated Driving

Faris Janjos¹, Maxim Dolgov¹, and J. Marius Zöllner²

Abstract—Making informed driving decisions requires reliable prediction of other vehicles’ trajectories. In this paper, we present a novel learned multi-modal trajectory prediction architecture for automated driving. It achieves kinematically feasible predictions by casting the learning problem into the space of accelerations and steering angles – by performing action-space prediction, we can leverage valuable model knowledge. Additionally, the dimensionality of the action manifold is lower than that of the state manifold, whose intrinsically correlated states are more difficult to capture in a learned manner. For the purpose of action-space prediction, we present the simple Feed-Forward Action-Space Prediction (FFW-ASP) architecture. Then, we build on this notion and introduce the novel Self-Supervised Action-Space Prediction (SSP-ASP) architecture that outputs future environment context features in addition to trajectories. A key element in the self-supervised architecture is that, based on an observed action history and past context features, future context features are predicted prior to future trajectories. The proposed methods are evaluated on real-world datasets containing urban intersections and roundabouts, and show accurate predictions, outperforming state-of-the-art for kinematically feasible predictions in several prediction metrics.

I. INTRODUCTION

Trajectory prediction is a crucial component of automated driving stacks. Its task is to digest traffic context information given in the form of raw sensor data or intermediate representations, in order to infer goals and intended motions of other traffic participants. Accurately predicting trajectories of surrounding agents is a prerequisite for downstream planning components, whose job is to navigate the autonomous vehicle reasonably and safely by executing high-level behavior plans and performing lower-level trajectory planning and vehicle control [1].

Predicting trajectories of human-driven vehicles shares complexities of understanding and predicting human motion in general [2]. Historically, most of the interest in human driving behavior and vehicle trajectory prediction has been shown in the context of driver assistance systems that employed classical robotics methods such as Kalman Filters (KF) [3], which perform well for short-term predictions but fail to capture intent-motivated long-term behavior. More information collected aboard vehicles, availability of large datasets, and the computing power of Graphics Processing Units (GPU) have driven the use of Deep Neural Networks (DNN) to achieve longer prediction horizons, as well as addressing full self-driving [4].

¹ Robert Bosch GmbH, Corporate Research, Advanced Autonomous Systems, 71272 Renningen, Germany. {faris.janjos, maxim.dolgov}@de.bosch.com

² Research Center for Information Technology (FZI), 76131 Karlsruhe, Germany. zoellner@fzi.de

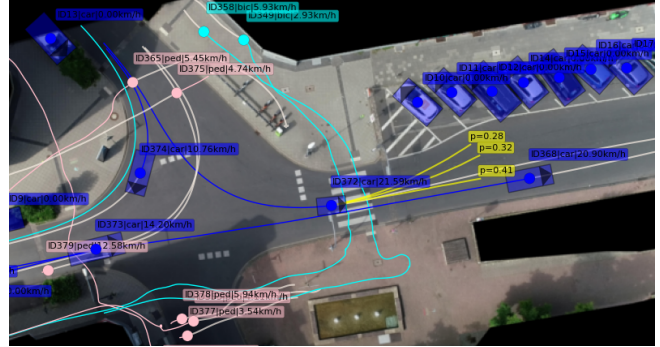


Fig. 1. Multi-modal trajectory prediction (yellow) trained on the inD dataset [6], using the SSP-ASP approach

Despite the large body of research, addressing vehicle trajectory prediction still remains a difficult problem to be solved especially for reasons such as complexity of understanding subtle social cues in multi-agent interactions and necessity of predicting multi-modal trajectories (see Fig. 1). Furthermore, many works neglect kinematic vehicle constraints in the framing of the learning problem [5]. Instead, the networks are tasked with capturing kinematic motion models in addition to the social and topological context by feeding inputs containing full vehicle states (position, heading, velocity, acceleration, etc.) and predicting future positions or waypoints as outputs.

In this work, we avoid these issues by constraining the learning problem to the action space and design architectures that benefit from such formulation. Our contributions are:

- We present a novel action-space learning paradigm, where the learning of motions is constrained purely to the action space of controlled accelerations and steering angles, both from the input and output sides. Position values or state values are then inferred via explicit kinematic motion models.
- A self-supervised action-based prediction architecture with several novel concepts:
 - Prediction of context features that are used for trajectory prediction
 - Reconstruction of action inputs using context features, helping the network learn a manifold sufficient for prediction of both features and trajectories
 - Long-term prediction (longer than 3s) by chaining two predicted segments, which can be regarded as a conceptual middle ground between autoregressive/single-step approaches and one-shot/multi-step approaches.

II. RELATED WORK

Learned models such as DNNs trained on large datasets of potentially high-dimensional data (real or simulated) have shown capability at tackling vehicle trajectory prediction. They perform combined reasoning about static environment information (e.g. geometric road structure) and dynamic multi-agent interaction to extract sufficient latent statistics necessary to infer reasonable future trajectories. Among these models, different deep architectures as well as their combinations are:

- *Convolutional Neural Networks (CNN)* [7] capture planar or spatial information from multi-channel images to construct locational visual features relevant to a scene.
- *Recurrent Neural Networks (RNN)* [7] naturally model the sequential nature of the prediction problem, since consecutive points of a trajectory are propagated in a recurrent manner.
- *Graph Neural Networks (GNN)* [8] encode geometric structure and interactions among different agents into an attention-based graph. By having lower-dimensional inputs than CNNs, large reductions in the number of model weights can be made. A special class are Graph Convolutional Networks (GCN), which employ so-called graph convolutions to extract richer topological representations than vanilla GNNs [9].

In relation to this distinction, a categorization by different input modalities to *raster-*, *polyline-*, or *sensor-based* approaches can be made. *Raster-based* approaches [10], [5], [11], [12], [13], [14] take in Bird’s Eye View (BEV) images of an agent’s environment with elements such as road lanes and bounding boxes of other perceived agents. By doing so, the CNN network can extract local spatial information from a single representational domain. Even though notions of distance are represented adequately, a large computational effort in training is needed to extract relevant features. In contrast, *polyline-based* approaches [15], [16], [9], [17] use GNNs that accept polylines or vectors representing surrounding roads and nearby agents. Another approach is predicting directly from sensor data such as LiDAR point clouds [18], [19], [20], [21], [22]. Such *sensor-based* approaches can perform object detection in addition to prediction, and propagate perception uncertainty throughout the pipeline. However, they require a very large computational effort in training and usually are not robust to sensor set changes.

More fundamentally, prediction approaches can be categorized by different learning paradigms that answer the question whether the prediction yields identical outputs given the same deterministic input data. Many *supervised-learning* approaches have consistent outputs given deterministic data – they either directly regress a trajectory [10], [5], or model uncertainty by predicting trajectories as sequences of means and covariances of positions, thus modeling the trajectories as uncorrelated distributions [12], [23], [24]. Similarly, some approaches improve prediction by performing classification over a predefined trajectory set [12], [14] or a target position set [16]. In contrast, *latent variable* approaches output ran-

dom values w.r.t. the same deterministic data, by sampling a latent distribution while inferring trajectory candidates [20], [21], [25], [26], [19]. For example [21] defines prediction in this setting as trajectory forecasting, a class of imitation learning with non-interaction. Such approaches usually incorporate probabilistic latent variable priors that capture uncertainty as a set of non-interpretable random variables, or leverage Generative Adversarial Networks (GAN) [27]. However, their major drawback is the reliance on sequential sampling, which accumulates errors in each step. A notable exception is [19], offering a high-dimensional continuous latent model employing GNN encoder and decoder networks.

Furthermore, approaches can be distinguished into two classes based on how a trajectory is generated: (i) *one-shot* prediction approaches [12], [10], [19] that output an entire trajectory and (ii) *single-step*, autoregressive approaches that build a trajectory sequentially [20], [21], [26]. According to how they model multi-agent interaction, most existing works perform prediction for each agent individually. Examples of these *single-agent* approaches are [10], [5], [12], [11]. Exceptions exist that consider the set of agents *jointly*, such as [26], [19], [21]. For example, [26] offers a discrete latent variable model with recurrent encoder and decoder networks, enabling joint prediction of all actors’ trajectories in a scene.

Because the agents’ true intentions are not known, trajectory predictions are inherently multi-modal. When it comes to modeling multi-modality, many *deterministic-mode* approaches directly predict multiple candidate trajectories along with their probabilities [10], [5]. Similarly, *Gaussian-mode* approaches represent a trajectory as a weighted mixture (each element is a candidate trajectory) of multi-variate Gaussians time-wise and predict means and variances [12], [28]. Alternatively, previously mentioned *sampling-based* approaches draw many samples from their decoder networks to obtain a notion of how likely a certain mode is. A notable class are *heuristics-based* approaches, which either train an additional network to predict an anchor trajectory from a set of heuristically chosen trajectories [12], [14], or use the road structure to infer viable target positions or regions [17], [16].

Many of the presented approaches can be abstracted to a duo of generic encoder/decoder networks (potentially with an additional prior network) with deterministic or random outputs, where backbone encoders compress the scene into features from which decoders infer trajectories. This assumes a complete reliance on learning to model physically feasible trajectory generation for the agent(s) of interest, which can be accurately described by a kinematic motion model instead. Such approaches opt to learn this model by reasoning about correlations among individual state variables, which in turn produces strong requirements on diversity in training data. A notable exception is [5], where a network learns action variables that are propagated through a bicycle model to infer trajectories. However, it achieves this by mapping states to actions, which assumes learning an inverse motion model instead. Similar approach that learns actions for prediction is [29], which employs a large set of manually designed situational features as inputs.

In our approach, we argue that combining learned and physical models, in addition to yielding kinematically feasible trajectories, improves robustness by uncoupling mode-able aspects from the learning task. To this end, we move the learning into the action space, by transforming action inputs to action outputs, and then use kinematic models to reconstruct trajectories. More fundamentally, action inputs in data are direct results of driver commands, as opposed to vehicle positions that are results of applied actions, and thus have the potential to model driving behavior more closely.

Learning action outputs is prevalent in end-to-end approaches such as [4], [30], [31]. An advantage of using action outputs for the prediction problem is that they allow to reason more closely about causal effects of actions on internal network representations. Practically, this can be achieved by principles of self-supervision, which is used in the context of representation learning for applications such as automatic label generation [32], [33]. However, it finds applications in imitation learning as well [34], [31]. Here, self-supervision usually entails learning forward and inverse transformations concurrently [34]. For example, if a certain action applied to a forward model results in an output described by generic features, it should be possible to reconstruct this applied action by feeding two consecutive features to an inverse model, whose job is to output actions. Inspired by these principles, we design a self-supervised trajectory prediction architecture, presented in Sec. IV-C.

III. PROBLEM DESCRIPTION

In general, trajectory prediction of human-driven vehicles can be framed in an imitation learning setting of modeling a distribution of trajectories \mathbf{Y} given data \mathcal{D}

$$\mathbf{Y} \sim P(\mathbf{Y}|\mathcal{D}) . \quad (1)$$

Data \mathcal{D} can include prior trajectory information of the vehicle for which prediction is done (prediction-ego), sensor data acquired from the environment, or any kind of stored knowledge such as map information. It is an established approach to introduce a categorical hidden variable – mode, and predict trajectories deterministically or as a probability distribution, conditioned on the mode. Then, in view of the *deterministic-mode* approaches mentioned in Sec. II, the problem in (1) can be simplified by predicting m modes of the distribution, i.e. deterministic trajectory Y_m and probability p_m pairs .

Trajectories Y can be defined in several ways – a vehicle’s position trajectory is a T -step sequence of planar coordinates $X_{1:T}$, where each X_t is represented by $[x, y]_t$. Similarly, we choose to define a full-state trajectory by the orientation and velocity in addition to positions; it is a sequence $S_{1:T}$, where S_t is $[x, y, \theta, v]_t$, and $X_{1:T} \subset S_{1:T}$. Additionally, we define an action trajectory $A_{1:T}$ as a sequence of controlled accelerations a_t and steering angles δ_t , where A_t is $[a, \delta]_t$. These action values fully capture the behavior of the driver along the time horizon $1 : T$ in a given driving situation.

More precisely, we are interested in inferring the future position trajectory $X_{1:T}$ for the prediction ego vehicle, given data \mathcal{D} that includes either past $X_{-T:0}$, $S_{-T:0}$, or

$A_{-T:0}$, as well as generic environment observations $O_{-T:0}$. Each O_t can contain observations in the form of LiDAR or BEV rasterized images of the vehicle’s surroundings, including road structure and other agents (vehicles, cyclists, pedestrians). In our implementation, we opt for rasterized BEV representations, as displayed in Fig. 5.

A. Action-space prediction

In action prediction, the task is to predict future driving actions $A_{1:T}$. Therefore, learned action-space prediction can be defined as a generic learned mapping of past actions (without past positions and states) and generic observations to future actions

$$\{A_{-T:0}, O_{-T:0}\} \mapsto A_{1:T} . \quad (2)$$

For simplicity, (2) only shows uni-modal action prediction, however a multi-modal extension to m action modes $A_{1:T,m}, p_m$ is straightforward.

Future position values $X_{1:T}$ are included in $S_{1:T}$, which is obtained by iteratively propagating actions $A_{1:T}$ through a kinematic motion model f

$$S_{t+1} = f(S_t, A_t) . \quad (3)$$

Kinematic models of reasonable complexity sufficiently approximate true vehicle motion. They are virtually always valid and the cases where they are wrong (e.g. skidding) are rare and easy to detect. We opt for the bicycle model [35], and perform the full state update in the following manner

$$\begin{aligned} x_{t+1} &= x_t + v_t \cos(\theta_t + \beta_t) \Delta T , \\ y_{t+1} &= y_t + v_t \sin(\theta_t + \beta_t) \Delta T , \\ \theta_{t+1} &= \theta_t + \frac{v_t}{l_r} \sin(\beta_t) \Delta T , \\ v_{t+1} &= v_t + a_t \Delta T , \\ \beta_t &= \tan^{-1} \left(\frac{l_r}{l_f + l_r} \tan \delta_t \right) . \end{aligned} \quad (4)$$

Here, ΔT is the sampling time, β is the angle between the center-of-mass velocity and the longitudinal axis of the car, while l_f and l_r are distances from the center of mass to the front and rear wheels. Similarly, we define an inverse bicycle model as a state-to-action mapping. Due to overdetermined (4), we choose to obtain the actions via v and θ

$$\begin{aligned} a_t &= \frac{v_{t+1} - v_t}{\Delta T} , \\ \delta_t &= \text{sgn} \left(\frac{\theta_{t+1} - \theta_t}{\bar{v}_t} \right) \arctan \left(\frac{l_f + l_r}{\sqrt{(\frac{\bar{v}_t}{\theta_{t+1} - \theta_t})^2 - l_r^2}} \right) , \end{aligned} \quad (5)$$

where $\bar{v}_t = \frac{v_t + v_{t+1}}{2}$. Identical inverse model is used in [29].

B. Learned mappings

In terms of modeling kinematic characteristics and while ignoring generic observations, the previously presented *action-to-action* mapping in (2) brings several benefits to the learning problem, contrary to learning *state-to-position* [10], *state-to-state* [11], or *state-to-action* [5] mappings:

- In a *state-to-position* or *state-to-state* mapping, the network has to implicitly capture a kinematic motion model (e.g. (4)) while reasoning about the correlation among individual states. To capture a valid model, a large number of diverse motions need to be present in the data (and not be underrepresented), such as driving straight, slight/sharp turns, U-turns, hard braking, etc.
- A *state-to-action* mapping, used in Deep Kinematic Models (DKM) approach [5], incorporates an explicit forward motion model (e.g. (4)) to obtain states from actions. However, the network still has to implicitly capture an inverse model (e.g. (5)) from sufficiently diverse data.
- An *action-to-action* mapping fully captures kinematic characteristics and reduces requirements on the motion representation in the data. Importantly, it is of lower dimensionality than *state-to-state* for instance, and makes capturing correlations between action variables easier.

Action-to-action prediction requires acceleration and steering angle values in tracked data, otherwise they can be inferred from states via inverse models such as (5). Examples of datasets where accelerations are provided are [6], [36].

IV. ACTION-SPACE PREDICTION METHODS

In this section, we present architectures that employ action-space prediction. We introduce the following notation:

- τ_0 is the past T -step time interval $[-T : 0]$
- τ_1 is the future T -step time interval $[1 : T + 1]$
- τ_2 is the future T -step time interval $[T + 2 : 2T + 2]$
- $\hat{\cdot}$ denotes predicted values
- $*$ denotes ground truth values

A. Feed-forward action-space prediction: FFW-ASP

The FFW-ASP architecture, shown in Fig. 2, realizes the mapping of past actions and observations to future actions (given in (2)) via the standard encoder/decoder architecture. It can be described by the following sequence of mappings

$$o_{\tau_0} \xrightarrow{\phi} z_{\tau_0}, \quad (6)$$

$$z_{\tau_0}, a_{\tau_0} \xrightarrow{\gamma} \hat{a}_{\tau_1}, \quad (7)$$

$$\hat{x}_{\tau_1} = f(\hat{a}_{\tau_1}, x_0), \quad (8)$$

where ϕ parameterizes an encoder network that maps past observations to features, and γ parameterizes a decoder that maps features and past actions to future actions. Future positions are obtained from (4) via the kinematic model $f(\cdot)$ that requires the present position x_0 in addition to future actions \hat{a}_{τ_1} , in order to reconstruct future positions \hat{x}_{τ_1} .

The loss function penalizes the difference between predicted positions and ground truth positions. In our implementation, we opt for the Huber loss with a cut-off at $h = 1.0$

$$\Delta x_{\tau_1} = \hat{x}_{\tau_1} - x_{\tau_1}^*,$$

$$\mathcal{L} = \|\Delta x_{\tau_1}\| = \begin{cases} \frac{1}{2} \Delta x_{\tau_1}^2, & |\Delta x_{\tau_1}| < h \\ h(|\Delta x_{\tau_1}| - \frac{1}{2}h), & \text{otherwise} \end{cases} \quad (9)$$

This loss function incorporates predicted positions obtained via the fully-differentiable kinematic model, making back-propagation possible.

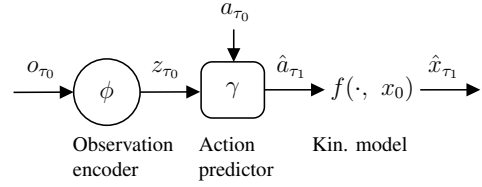


Fig. 2. FFW-ASP architecture: encoder with parameters ϕ accepts a history of observations o_{τ_0} and generates features z_{τ_0} . Then, a decoder with parameters γ combines features z_{τ_0} with action history a_{τ_0} to generate future actions \hat{a}_{τ_1} . Kinematic model $f(\cdot, x_0)$ reconstructs a position trajectory

It is straightforward to extend this architecture to multi-modal predictions. Inspired by [10], the action decoder can be adapted to predict M action trajectories $\hat{a}_{\tau_1, m}$ along with their probabilities p_m , where $m \in \{1, \dots, M\}$. In this case, the loss function is extended with a binary indicator function I and a cross-entropy loss term

$$\mathcal{L}_{FFW} = \sum_{m=1}^M I_{m=m^\dagger} (\|\Delta x_{\tau_1, m}\|) - \frac{\exp(p_{m^\dagger})}{\sum_m \exp(p_m)}, \quad (10)$$

where the indicator selects the mode closest to the ground-truth (denoted by \dagger), while the cross-entropy term rewards confidence in the chosen mode. The mode-to-ground-truth distance uses a combination of angle difference between the last points of the two trajectories and L_2 distance between each point [10].

This simple feed-forward architecture capitalizes on the benefits of *action-to-action* mappings from Sec. III-A. In the next section, we describe the methodology of self-supervision in an action-based context, before presenting a self-supervised trajectory prediction architecture.

B. Self-supervision background

The forward and inverse transformations in the context of self-supervision, previously mentioned in Sec. II, have been used in robotic manipulation tasks [34] to jointly learn mappings from visual features generated from images of objects to physical robot actions on the objects and vice-versa. This architecture has been adapted for end-to-end driving in [31], where a pre-trained self-supervised forward/inverse model outperforms pure end-to-end models that map images to driving actions. Furthermore, a categorization of different learned transformations is offered in [31], which we summarize here with one-step predictions.

- 1) **Behavioral cloning** models map an observation to latent features with a ϕ -encoder, and map features to action output with a γ -decoder

$$o_t \xrightarrow{\phi} z_t \xrightarrow{\gamma} \hat{a}_t. \quad (11)$$

The loss is a difference between the label and the output

$$\mathcal{L}_{BC} = \|a_t^* - \hat{a}_t\|. \quad (12)$$

- 2) **Inverse** models encode observations into features at two successive time-steps. Then, they learn a ξ -parameterized mapping from two consecutive features

to an action, to reconstruct the applied action that resulted in a new observation

$$\left. \begin{array}{l} o_t \xrightarrow{\phi} z_t \\ o_{t+1} \xrightarrow{\phi} z_{t+1} \end{array} \right\} \xrightarrow{\xi} \hat{a}_t, \quad (13)$$

with a reconstruction loss

$$\mathcal{L}_{INV} = \|a_t^* - \hat{a}_t\|. \quad (14)$$

- 3) **Forward** models, parameterized by ψ , predict the new latent features given past features and action

$$\left. \begin{array}{l} o_t \xrightarrow{\phi} z_t \\ a_t \end{array} \right\} \xrightarrow{\psi} \hat{z}_{t+1}, \quad (15)$$

$$o_{t+1} \xrightarrow{\phi} z_{t+1}. \quad (16)$$

Optimizing only the feature mismatch between the predicted future features \hat{z}_{t+1} and the encoded features z_{t+1} can lead to networks outputting the trivial solution of zero features. Therefore, a regularization term is added in the form of the inverse model loss (14)

$$\mathcal{L}_{FW} = \|z_{t+1} - \hat{z}_{t+1}\| + \|a_t^* - \hat{a}_t\|. \quad (17)$$

The regularized forward model is preferable to pure behavioral cloning, since the networks gain a richer understanding of the interplay between actions and features. The model can reconstruct its inputs, as well as predict its internal representation of the environment (in the form of features), as opposed to predicting observations directly, which can be infeasible in the case of camera images for example.

C. Self-supervised action-space prediction: SSP-ASP

The previously presented forward model (with an inverse model regularizer) predicts only future latent features. In order to use it for trajectory prediction, we add an action predictor component parameterized by γ

$$a_t, z_t, \{z_{t+1}, \hat{z}_{t+1}\} \xrightarrow{\gamma} \hat{a}_{t+1}. \quad (18)$$

This mapping predicts the future action \hat{a}_{t+1} by combining the known past action a_t , encoded past latent feature z_t , and one of the future features $\{z_{t+1}, \hat{z}_{t+1}\}$. The difference is that z_{t+1} is used at training time and obtained via the encoding ϕ (16), while \hat{z}_{t+1} is used at inference time and obtained via the prediction ψ (15). With the additional action predictor, the total self-supervised action prediction loss extends the regularized forward model loss (17) according to

$$\mathcal{L} = \|z_{t+1} - \hat{z}_{t+1}\| + \|a_t - \hat{a}_t\| + \|a_{t+1}^* - \hat{a}_{t+1}\|. \quad (19)$$

In summary, it incorporates the forward model that predicts future features (feature predictor), the inverse model regularizer that ‘predicts’ the past actions (action reconstructor), and the action predictor, predicting future actions.

The complete procedure to obtain the training loss (19) is visualized in Fig. 3 for T -step intervals. First, we encode observations from past and future intervals o_{τ_0} and o_{τ_1} separately into features z_{τ_0} and z_{τ_1} . Then, we reconstruct the past action by generating \hat{a}_{τ_0} while simultaneously predicting future features \hat{z}_{τ_1} . Finally, we predict future actions \hat{a}_{τ_1} using a_{τ_0} , z_{τ_0} , and z_{τ_1} (in training) or \hat{z}_{τ_1} (during inference).

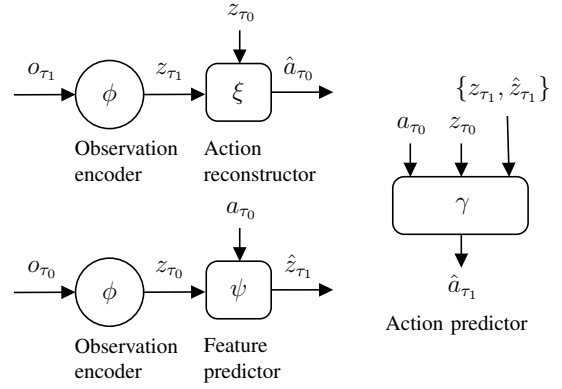


Fig. 3. SSP-ASP training architecture: encoder with parameters ϕ accepts observations at two consecutive intervals o_{τ_0} and o_{τ_1} separately, generates features z_{τ_0} and z_{τ_1} , and then the action reconstructor ξ and feature predictor ψ reconstruct past actions \hat{a}_{τ_0} and predict future features \hat{z}_{τ_1} , respectively. The action predictor uses past actions a_{τ_0} and consecutive features z_{τ_0} and z_{τ_1} (or \hat{z}_{τ_1}) to predict future actions \hat{a}_{τ_1} . Kinematic transformation is omitted for clarity.

In practice, we run the action predictor with both encoded and predicted features in training – we use both outputs in the loss, in order to avoid a distribution mismatch during inference. For inference, the architecture in Fig. 3 reduces to encoding only past observation o_{τ_0} (since o_{τ_1} is not available), predicting features \hat{z}_{τ_1} , and then predicting future actions \hat{a}_{τ_1} using a_{τ_0} , z_{τ_0} , and \hat{z}_{τ_1} . Finally, since we are interested in multi-modal position prediction over a T -step interval as opposed to a single time-step, (19) becomes

$$\begin{aligned} \mathcal{L}_{SSP} = & w_1 \|a_{\tau_0} - \hat{a}_{\tau_0}\| + w_2 \|z_{\tau_1} - \hat{z}_{\tau_1}\| + \\ & w_3 \sum_{m=1}^M I_{m=m^\dagger} (\|\Delta x_{\tau_1, m}\|) - w_4 \frac{\exp(p_{m^\dagger})}{\sum_m \exp(p_m)}. \end{aligned} \quad (20)$$

Here, the weights $\{w_i\}_{i=1}^4$ penalize action reconstruction, feature mismatch, multi-modal regression, and classification.

An important aspect of the self-supervised action prediction problem is its time-interval formulation. It enables us to introduce a distinction between *single-segment* prediction, and a long-term, *multi-segment* prediction.

1) *Single-segment prediction*: We have so far considered the same T -step time interval for all the past and future values. In this setup, we predict a single segment of values of interest, exemplified in Fig. 3, with the constraint of same time interval length for the past and future. The duration can be regarded as a design choice. We opt for 3s segment length since we assume that [-3:0]s history is long enough to capture relevant scene context, and [0:3]s future is a meaningful, albeit not long-term, prediction interval.

2) *Multi-segment prediction*: The self-supervised architecture makes it possible to chain several predicted segments and achieve long-term prediction. This can be done both in training and inference by additionally generating features and actions along the τ_2 interval. The inference architecture is visualized in Fig. 4. Here, the feature predictor ψ is run once more to obtain \hat{z}_{τ_2} , and action predictor γ to obtain \hat{a}_{τ_2} . For the 3s segment length it would constitute a prediction on

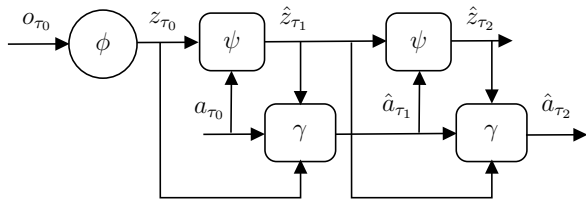


Fig. 4. SSP-ASP two-segment *inference* architecture: encoder with parameters ϕ accepts observations o_{τ_0} and then alternately, future features \hat{z}_{τ_1} and \hat{z}_{τ_2} , and actions \hat{a}_{τ_1} and \hat{a}_{τ_2} are generated. First, \hat{z}_{τ_1} and \hat{a}_{τ_1} are generated with the help of encoded features z_{τ_0} , and then, \hat{z}_{τ_2} and \hat{a}_{τ_2} with the help of predicted features \hat{z}_{τ_1} . Note how the action reconstructor ξ from Fig. 3 is not needed in inference.

the [3:6]s interval. The training case is similar to Fig. 3, with o_{τ_1} and o_{τ_2} as inputs. The same procedure is carried out, obtaining encoded features z_{τ_1} and z_{τ_2} , and predicting \hat{z}_{τ_2} . Finally, \hat{a}_{τ_2} can be obtained either with the encoded z_{τ_2} or the predicted \hat{z}_{τ_2} . In general, the multi-segment chaining can be performed with the same procedure for even more segments further into the future. In our implementation, we focus on two segments.

Multi-segment prediction requires non-trivial chaining of multi-modal trajectories. For example, the predicted action output along τ_1 is multi-modal with m modes, and it needs to be fed again into the action predictor γ that accepts unimodal inputs, and outputs multi-modal actions along τ_2 . Naturally, it is possible to feed m modes individually and obtain m^2 chained trajectories at the output, requiring a large computational effort both in training and inference. A less costly alternative is feeding the highest probability trajectory within the multi-modal actions. Similarly, *label matching* can be done – the action mode closest to the label position trajectory can be chosen (after a kinematic transform of the actions), with the distance metric the same as in the regression component of the losses (10) and (20). In this context, label matching can be regarded as a variant of guided teacher forcing [37] – a method to accelerate training of RNNs by replacing the outputs of earlier stages of the network with ground truth samples.

In the context of prediction, the self-supervised architectures in Fig. 3 and Fig. 4 improve on classic encoder-decoder setups exemplified by Fig. 2. They achieve this by incorporating future observations in training, as opposed to only past observations, while at the same time predicting the future context and reconstructing the past actions. This joint learning helps all the networks form richer representations.

V. RESULTS

In this section, we describe the implementation details of the approach proposed in Sec. IV. We specify the training procedure, the datasets that were used for training, and present the obtained results.

A. Implementation

In Sec. IV, we have assumed generic observations as inputs to generic encoder networks that can reason with different input representations (as categorized in Sec. II).

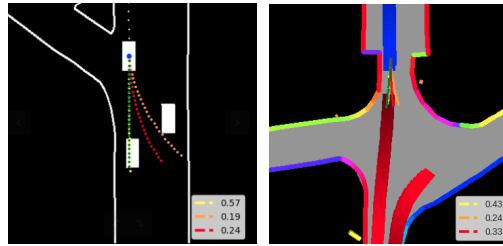


Fig. 5. Example predicted trajectories with ChauffeurNet (all channels superimposed) and MTP rasters on inD [6]; green trajectory indicates ground truth, while red, orange, and yellow trajectories are predicted modes

In our implementation, we opt for *raster-based* images and work with two variants visualized in Fig. 5. The first variant is a sparse black and white 12-channel 360x240 representation, similar to the ChauffeurNet representation [13]. Here, individual channels contain the road boundary polylines, prediction-ego bounding box, prediction-ego trajectory history, and multiple snapshots (sampled at regular time-intervals) of bounding boxes of all traffic agents. The second variant is a 3-channel 360x360 RGB-image similar to the Multi-Modal Trajectory Prediction (MTP) representation [10]. Here, the road boundary polylines, drivable areas, and prediction-ego and traffic bounding boxes are overlaid on a single image, where different semantics have specific color values. We implemented this variant with the help of nuScenes devkit [38].

The rasterized inputs are fed into ResNet18 [39] encoder backbone networks returning a 512-sized feature vector, both for the case of feed-forward and self-supervised architectures. For the former, the γ action predictor (Fig. 2) is realized as a 2-layer Gated Rectifier Unit (GRU) with 512 hidden units. For the self-supervised architecture (Fig. 3), we use the following networks: feature predictor ψ and the action predictor γ are also 2-layer GRUs with 512 hidden units, whereas the action reconstructor ξ is a Multilayer Perceptron (MLP) with layer sizes $\{256, 128, 64\}$. The γ and ξ networks output acceleration and steering angle values in the range $[-1, 1]$, which are then scaled to the range observed in the dataset.

In both feed-forward and self-supervised architectures we consider a 3s history and observe two use-cases: predicting a 3s and a 6s trajectory. For the 6s prediction, the trajectory is generated via two different prediction paradigms: one-shot prediction for the feed-forward architecture and chaining two 3s predictions for the self-supervised architecture (with label matching to account for multi-modality).

B. Datasets

We evaluated our approach on two real-world datasets recorded on German roads: inD (urban intersections) [6] and roundD (roundabouts) [36]. In total, they contain highly accurate drone-recorded trajectories of over 25000 agents of different classes, such as cars, trucks, buses, motorcycles, cyclists, and pedestrians. We performed prediction for all agent classes except cyclists and pedestrians. A drawback of the datasets is the lack of signalized intersections, which

were not considered in our approach but can be easily integrated into the input representation. For example, the ChauffeurNet [13] rasterization considers traffic light status as an additional channel.

Depending on the prediction horizon, we extracted all 3+3s (3s past and 3s prediction) or 3+6s (3s past and 6s prediction) trajectory snippets from the datasets, with a 0.6s spacing. We split each dataset into training, validation, and testing subsets according to an 8:1:1 ratio, with each subset containing recordings taken at a different time of the day, thus ensuring no overlap. To generate the road boundaries polylines, we used the provided lanelet maps [40].

C. Training setup

The feed-forward and self-supervised architectures were trained on the accompanying losses (10) and (20). For the self-supervised case, we used equal weighting for the loss components. Similarly to (10), each loss component is represented by the Huber loss function (9).

The self-supervised architecture offers great flexibility in different ways to pre-train the models. We experimented with training on only the action reconstruction and feature mismatch loss components from (20) prior to the full loss, essentially implementing (17). We observed that this *forward-model pre-training* improves performance since it enables the features to be learned to a certain degree before the actual prediction is performed. Additionally, in the 6s prediction horizon case, we observed performance gains by loading and retraining a model used for 3s prediction.

All models were implemented in PyTorch [41] and trained on two NVIDIA GeForce GTX 1080 GPUs using the Adam optimizer [42], a batch size of 32, and 10 epochs. The learning rate was set to 10^{-4} and reduced by a factor of five if the validation loss did not improve over three consecutive epochs. In self-supervised prediction, we performed additional forward-model pre-training over 3 epochs.

D. Performance

We evaluated the performance of our FFW-ASP (Sec. IV-A) and SSP-ASP (Sec. IV-B) approaches on inD [6] and rounD [36] datasets. We benchmarked them against DKM [5], another method that achieves kinematically feasible predictions, albeit by using a *state-to-action* mapping introduced in Sec. III-B compared to our proposed *action-to-action* mapping. This method improves on the authors’ prior work [10], whose multi-modality concept and rasterization we leverage. All methods were compared in both ChauffeurNet [13] and MTP [10] rasterization setups. For a fair comparison, we used a ResNet18 encoder in all setups and performed 3s and 6s prediction based on a 3s history (with 3 modes). As evaluation metrics, we calculated the Mean Absolute Error (MAE)¹, Mean Squared Error (MSE)², and Final Displacement Error (FDE)³ to the ground-truth on the testing datasets.

¹mean $L1$ distance across all time-steps

²mean $L2$ distance across all time-steps

³ $L2$ distance at final time-step

inD		3s			6s		
		MAE	MSE	FDE	MAE	MSE	FDE
Chauffeur Net	DKM	0.48	0.86	2.01	1.27	7.44	5.91
	FFW-ASP	0.27	0.33	1.23	1.13	6.42	5.45
	SSP-ASP	0.21	0.24	0.98	1.23	6.52	5.15
MTP	DKM	0.58	1.19	2.36	1.34	7.89	6.29
	FFW-ASP	0.30	0.39	1.41	1.19	6.78	5.72
	SSP-ASP	0.22	0.25	1.04	1.15	6.08	5.02

rounD		3s			6s		
		MAE	MSE	FDE	MAE	MSE	FDE
Chauffeur Net	DKM	0.29	0.29	1.12	1.35	7.22	5.55
	FFW-ASP	0.22	0.18	0.93	1.12	6.17	5.08
	SSP-ASP	0.17	0.12	0.73	1.34	6.44	4.69
MTP	DKM	0.29	0.28	1.22	1.25	6.13	5.51
	FFW-ASP	0.22	0.18	0.94	1.08	5.84	4.76
	SSP-ASP	0.17	0.12	0.74	1.25	7.08	4.61

TABLE I

RESULTS OBTAINED ON THE IND [6] AND ROUND [36] DATASETS

The results are provided in Tab. I, showing that FFW-ASP already brings improvements over DKM on both datasets. Since the two approaches differ in the choice of the prediction head network (DKM has a fully connected layer, while FFW-ASP has a GRU), we tested FFW-ASP using a DKM prediction head and still achieved improvements (omitted in the table). Furthermore, SSP-ASP offers clear improvements to FFW-ASP on both datasets for 3s prediction, while for 6s prediction the feed-forward architecture achieves similar results overall. This indicates that the method of chaining multi-modal trajectories, specific to the multi-segment variant, could potentially be improved. Nevertheless, SSP-ASP achieves the lowest FDE across all settings.

VI. CONCLUSION

In this paper, we offered an action-based perspective into the problem of vehicle trajectory prediction. Results indicate that uncoupling modelable aspects from the learning problem, such as learning forward and inverse motion models, improves prediction performance while ensuring kinematic feasibility. As a main result, we proposed a novel self-supervised action-based architecture for prediction. By predicting future latent features and reconstructing past actions simultaneously, we capture the interplay between actions and their effects on the networks’ internal representations. We extract more information by leveraging future observations in training, which we use to predict future latent features – a feasible alternative to predicting observations. Finally, we achieve long-term prediction via a new paradigm: in contrast to one-shot or single-step prediction approaches, we obtain a trajectory by chaining individual trajectory segments.

In future work, we plan to replace the computationally intensive CNN encoder with a lightweight GNN, as this is currently the bottleneck of the self-supervised approach. We expect more robust feature representation and thus a performance improvement, since the network would not have to extract objects from pixels. Furthermore, we would like to analyze the effects of time segment length on prediction quality. It remains to be seen whether shorter or longer segments can capture more latent information in a scene and whether chaining more than two segments could potentially achieve prediction horizons longer than 6s.

REFERENCES

- [1] B. Paden, M. Čáp, S. Z. Yong, D. Yershov, and E. Frazzoli, "A Survey of Motion Planning and Control Techniques for Self-Driving Urban Vehicles," *IEEE Transactions on Intelligent Vehicles*, vol. 1, no. 1, 2016.
- [2] A. Rudenko, L. Palmieri, M. Herman, K. M. Kitani, D. M. Gavrila, and K. O. Arras, "Human Motion Trajectory Prediction: A Survey," *The International Journal of Robotics Research*, vol. 39, no. 8, 2020.
- [3] S. Lefèvre, D. Vasquez, and C. Laugier, "A Survey on Motion Prediction and Risk Assessment for Intelligent Vehicles," *ROBOMECH Journal*, vol. 1, no. 1, 2014.
- [4] A. Tampuu, M. Semikin, N. Muhammad, D. Fishman, and T. Matisen, "A Survey of End-to-End Driving: Architectures and Training Methods," *arXiv preprint arXiv:2003.06404*, 2020.
- [5] H. Cui, T. Nguyen, F.-C. Chou, T.-H. Lin, J. Schneider, D. Bradley, and N. Djuric, "Deep Kinematic Models for Physically Realistic Prediction of Vehicle Trajectories," *arXiv preprint arXiv:1908.00219*, 2019.
- [6] J. Bock, R. Krajewski, T. Moers, S. Runde, L. Vater, and L. Eckstein, "The inD Dataset: A Drone Dataset of Naturalistic Road User Trajectories at German Intersections," *arXiv preprint arXiv:1911.07602*, 2019.
- [7] Y. LeCun, Y. Bengio, and G. Hinton, "Deep Learning," *Nature*, vol. 521, no. 7553, 2015.
- [8] F. Scarselli, M. Gori, A. C. Tsoi, M. Hagenbuchner, and G. Monfardini, "The Graph Neural Network Model," *IEEE Transactions on Neural Networks*, vol. 20, no. 1, 2008.
- [9] M. Liang, B. Yang, R. Hu, Y. Chen, R. Liao, S. Feng, and R. Urtasun, "Learning Lane Graph Representations for Motion Forecasting," in *European Conference on Computer Vision*. Springer, 2020.
- [10] H. Cui, V. Radosavljevic, F.-C. Chou, T.-H. Lin, T. Nguyen, T.-K. Huang, J. Schneider, and N. Djuric, "Multimodal Trajectory Predictions for Autonomous Driving Using Deep Convolutional Networks," in *2019 International Conference on Robotics and Automation (ICRA)*. IEEE, 2019.
- [11] J. Strohecker, V. Belagiannis, J. Müller, M. Schreiber, M. Herrmann, D. Wolf, and M. Buchholz, "Multiple Trajectory Prediction with Deep Temporal and Spatial Convolutional Neural Networks," in *2020 International Conference on Intelligent Robots and Systems (IROS)*. IEEE/RSJ, 2020.
- [12] Y. Chai, B. Sapp, M. Bansal, and D. Anguelov, "Multipath: Multiple Probabilistic Anchor Trajectory Hypotheses for Behavior Prediction," *arXiv preprint arXiv:1910.05449*, 2019.
- [13] M. Bansal, A. Krizhevsky, and A. Ogale, "ChauffeurNet: Learning to Drive by Imitating the Best and Synthesizing the Worst," *arXiv preprint arXiv:1812.03079*, 2018.
- [14] T. Phan-Minh, E. C. Grigore, F. A. Boulton, O. Beijbom, and E. M. Wolff, "Covnet: Multimodal Behavior Prediction Using Trajectory Sets," in *Proceedings of the IEEE/CVF Conference on Computer Vision and Pattern Recognition*, 2020.
- [15] J. Gao, C. Sun, H. Zhao, Y. Shen, D. Anguelov, C. Li, and C. Schmid, "VectorNet: Encoding HD Maps and Agent Dynamics from Vectorized Representation," in *Proceedings of the IEEE/CVF Conference on Computer Vision and Pattern Recognition*, 2020.
- [16] H. Zhao, J. Gao, T. Lan, C. Sun, B. Sapp, B. Varadarajan, Y. Shen, Y. Shen, Y. Chai, C. Schmid, *et al.*, "TNT: Target-driveN Trajectory Prediction," *arXiv preprint arXiv:2008.08294*, 2020.
- [17] S. Khandelwal, W. Qi, J. Singh, A. Hartnett, and D. Ramanan, "What-If Motion Prediction for Autonomous Driving," *arXiv preprint arXiv:2008.10587*, 2020.
- [18] S. Casas, W. Luo, and R. Urtasun, "IntentNet: Learning to Predict Intention from Raw Sensor Data," in *Conference on Robot Learning*, 2018.
- [19] S. Casas, C. Gulino, S. Suo, K. Luo, R. Liao, and R. Urtasun, "Implicit Latent Variable Model for Scene-Consistent Motion Forecasting," *arXiv preprint arXiv:2007.12036*, 2020.
- [20] N. Rhinehart, K. M. Kitani, and P. Vernaza, "R2P2: A Reparameterized Pushforward Policy for Diverse, Precise Generative Path Forecasting," in *Proceedings of the European Conference on Computer Vision (ECCV)*, 2018.
- [21] N. Rhinehart, R. McAllister, K. Kitani, and S. Levine, "PRECOG: Prediction Conditioned on Goals in Visual Multi-Agent Settings," in *Proceedings of the IEEE International Conference on Computer Vision*, 2019.
- [22] M. Liang, B. Yang, W. Zeng, Y. Chen, R. Hu, S. Casas, and R. Urtasun, "PnPNet: End-to-End Perception and Prediction with Tracking in the Loop," in *Proceedings of the IEEE/CVF Conference on Computer Vision and Pattern Recognition*, 2020.
- [23] N. Djuric, V. Radosavljevic, H. Cui, T. Nguyen, F.-C. Chou, T.-H. Lin, N. Singh, and J. Schneider, "Uncertainty-Aware Short-Term Motion Prediction of Traffic Actors for Autonomous Driving," in *Proceedings of the IEEE/CVF Winter Conference on Applications of Computer Vision*, 2020.
- [24] N. Djuric, H. Cui, Z. Su, S. Wu, H. Wang, F.-C. Chou, L. S. Martin, S. Feng, R. Hu, Y. Xu, *et al.*, "MultiNet: Multiclass Multistage Multimodal Motion Prediction," *arXiv preprint arXiv:2006.02000*, 2020.
- [25] N. Rhinehart, R. McAllister, and S. Levine, "Deep Imitative Models for Flexible Inference, Planning, and Control," *arXiv preprint arXiv:1810.06544*, 2018.
- [26] C. Tang and R. R. Salakhutdinov, "Multiple Futures Prediction," in *Advances in Neural Information Processing Systems*, 2019.
- [27] X. Huang, S. G. McGill, J. A. DeCastro, B. C. Williams, L. Fletcher, J. J. Leonard, and G. Rosman, "Diversity-Aware Vehicle Motion Prediction via Latent Semantic Sampling," *arXiv preprint arXiv:1911.12736*, 2019.
- [28] J. Hong, B. Sapp, and J. Philbin, "Rules of the Road: Predicting Driving Behavior with a Convolutional Model of Semantic Interactions," in *Proceedings of the IEEE/CVF Conference on Computer Vision and Pattern Recognition*, 2019.
- [29] J. Schulz, C. Hubmann, N. Morin, J. Löchner, and D. Burschka, "Learning Interaction-Aware Probabilistic Driver Behavior Models from Urban Scenarios," in *2019 IEEE Intelligent Vehicles Symposium (IV)*. IEEE, 2019.
- [30] M. Bojarski, D. Del Testa, D. Dworakowski, B. Firner, B. Flepp, P. Goyal, L. D. Jackel, M. Monfort, U. Muller, J. Zhang, *et al.*, "End-to-end Learning for Self-Driving Cars," *arXiv preprint arXiv:1604.07316*, 2016.
- [31] Y. Xiao, F. Codevilla, C. Pal, and A. M. Lopez, "Action-Based Representation Learning for Autonomous Driving," *arXiv preprint arXiv:2008.09417*, 2020.
- [32] A. Kolesnikov, X. Zhai, and L. Beyer, "Revisiting Self-Supervised Visual Representation Learning," in *Proceedings of the IEEE Conference on Computer Vision and Pattern Recognition*, 2019.
- [33] P. Goyal, D. Mahajan, A. Gupta, and I. Misra, "Scaling and Benchmarking Self-Supervised Visual Representation Learning," in *Proceedings of the IEEE International Conference on Computer Vision*, 2019.
- [34] P. Agrawal, A. V. Nair, P. Abbeel, J. Malik, and S. Levine, "Learning to Poke by Poking: Experiential Learning of Intuitive Physics," in *Advances in Neural Information Processing Systems*, 2016.
- [35] J. Kong, M. Pfeiffer, G. Schilbach, and F. Borrelli, "Kinematic and Dynamic Vehicle Models for Autonomous Driving Control Design," in *2015 IEEE Intelligent Vehicles Symposium (IV)*. IEEE, 2015.
- [36] R. Krajewski, T. Moers, J. Bock, L. Vater, and L. Eckstein, "The roundD Dataset: A Drone Dataset of Road User Trajectories at Roundabouts in Germany," in *2020 IEEE 23rd International Conference on Intelligent Transportation Systems (ITSC)*. IEEE, 2020, pp. 1–6.
- [37] R. J. Williams and D. Zipser, "A Learning Algorithm for Continually Running Fully Recurrent Neural Networks," *Neural Computation*, vol. 1, no. 2, 1989.
- [38] H. Caesar, V. Bankiti, A. H. Lang, S. Vora, V. E. Liong, Q. Xu, A. Krishnan, Y. Pan, G. Baldan, and O. Beijbom, "nuScenes: A Multimodal Dataset for Autonomous Driving," *arXiv preprint arXiv:1903.11027*, 2019.
- [39] K. He, X. Zhang, S. Ren, and J. Sun, "Deep Residual Learning for Image Recognition," in *Proceedings of the IEEE Conference on Computer Vision and Pattern Recognition*, 2016.
- [40] F. Poggendorf, J.-H. Pauls, J. Janosovits, S. Orf, M. Naumann, F. Kuhnt, and M. Mayr, "Lanelet2: A High-Definition Map Framework for the Future of Automated Driving," in *2018 21st International Conference on Intelligent Transportation Systems (ITSC)*. IEEE, 2018.
- [41] A. Paszke, S. Gross, F. Massa, A. Lerer, J. Bradbury, G. Chanan, T. Killeen, Z. Lin, N. Gimelshein, L. Antiga, *et al.*, "PyTorch: An Imperative Style, High-Performance Deep Learning Library," *arXiv preprint arXiv:1912.01703*, 2019.
- [42] D. P. Kingma and J. Ba, "Adam: A Method for Stochastic Optimization," *arXiv preprint arXiv:1412.6980*, 2014.